CHEMISTRY
A EUROPEAN JOURNAL

DOI: 10.1002/chem.200401312

Solid Film versus Solution-Phase Charge-Recombination Dynamics of exTTF–Bridge–C_{60} Dyads**

Samantha Handa,[a] Francesco Giacalone,[b] Saif A. Haque,[a] Emilio Palomares,*[a, c] Nazario Martín,*[b] and James R. Durrant[a]

Abstract: The charge-recombination dynamics of two exTTF–C_{60} dyads (exTTF = 9,10-bis(1,3-dithiol-2-ylidene)-9,10-dihydroanthracene), observed after photoinduced charge separation, are compared in solution and in the solid state. The dyads differ only in the degree of conjugation of the bridge between the donor (exTTF) and the acceptor (C_{60}) moieties. In solution, photoexcitation of the nonconjugated dyad C_{60}–BN–exTTF (**1**) (BN = 1,1′-binaphthyl) shows slower charge-recombination dynamics compared with the conjugated dyad C_{60}–TVB–exTTF (**2**) (TVB = bisthienylvinylenebenzene) (lifetimes of 24 and 0.6 μs, respectively), consistent with the expected stronger electronic coupling in the conjugated dyad. However, in solid films, the dynamics are remarkably different, with dyad **2** showing slower recombination dynamics than **1**. For dyad **1**, recombination dynamics for the solid films are observed to be tenfold faster than in solution, with this acceleration attributed to enhanced electronic coupling between the geminate radical pair in the solid film. In contrast, for dyad **2**, the recombination dynamics in the solid film exhibit a lifetime of 7 μs, tenfold slower than that observed for this dyad in solution. These slow recombination dynamics are assigned to the dissociation of the initially formed geminate radical pair to free carriers. Subsequent trapping of the free carriers at film defects results in the observed slow recombination dynamics. It is thus apparent that consideration of solution-phase recombination data is of only limited value in predicting the solid-film behaviour. These results are discussed with reference to the development of organic solar cells based upon molecular donor–acceptor structures.

Keywords: C_{60} dyads · donor–acceptor systems · electron transfer · self-assembly · thin films

Introduction

The achievement of ultrafast photoinduced electron transfer from conjugated polymers to C_{60} moieties has led to novel approaches for the fabrication of photovoltaic devices. Organic photovoltaic devices based upon an interpenetrating network of light-absorbing semiconducting polymer and electron-accepting C_{60}-derivative materials have resulted in device efficiencies in excess of approximately 3%.[1] At present, such interpenetrating networks typically comprise a random blending of the electron-donor and -acceptor species, with blend-morphology optimisation largely achieved through empirical correlations between film-deposition conditions and device performance. Control of this blend morphology on the nanometer scale is essential to achieve efficient charge separation and charge transport to the device contacts, whilst at the same time minimising interfacial charge-recombination losses. There is therefore considerable interest in developing approaches to control the morphology of the materials on the nanoscale. One elegant approach to

[a] S. Handa, S. A. Haque, Dr. E. Palomares, J. R. Durrant
Centre for Electronic Material and Devices
Department of Chemistry, Imperial College
Exhibition Road, South Kensington, SW7 2AZ, London (UK)
Fax: (+44) 207-594-5801
E-mail: emilio.palomares@uv.es

[b] F. Giacalone, N. Martín
Departamento de Química Orgánica
Facultad de Ciencias Químicas
Universidad Complutense, 28040 Madrid (Spain)
Fax: (+34) 91-394-4103
E-mail: nazmar@quim.ucm.es

[c] Dr. E. Palomares
Present address: Institut de Ciencia Molecular (IcMol)
Universitat de Valencia, 46100 Burjassot, Valencia (Spain)
Fax: (+34) 96-354-4859

[**] exTTF = 9,10-bis(1,3-dithiol-2-ylidene)-9,10-dihydroanthracene, that is, π-extended tetrathiafulvalene.

this problem that is currently receiving attention is the use of supermolecular donor–acceptor dyads. In such dyads, the donor and acceptor species are covalently bound, attached by a suitable molecular bridge such as to allow charge separation whilst minimising the charge-recombination back reaction.[2–4] Further studies have addressed the potential for engineering such dyads to allow self-assembly and form ordered solid-state materials.[5,6]

Supermolecular and supramolecular donor–acceptor structures have been widely studied in solution as simple model systems for studies of photoinduced electron-transfer dynamics.[7,8] Careful design of molecular structure has led to near-unity charge-separation yields, with lifetimes of the charge-separated state of up to hundreds of microseconds, even for simple dyad structures.[9–11] Moreover, this molecular approach has been employed for photochemical energy conversion including, for example, the harnessing of solar irradiation for the generation of adenosine triphosphate (ATP) in solution.[12] However, the application of such molecular structures to organic photovoltaics requires consideration and optimisation of their behaviour in solid films. Several studies have addressed the photovoltaic performance of organic thin films fabricated from C_{60}–OPV (fullerene–oligo(phenylenevinylene))[13–20] and C_{60}–OPE (fullerene–oligo(phenyleneethynylene))[21,22]conjugates and double cables. However, only very modest device efficiencies were achieved that were attributed to excessive charge-recombination losses.[10]

Recently, Janssen et al. have reported a comparison of electron-transfer dynamics for a C_{60}–OPV dyad in solution and as a solid film.[23] This study focused on the ultrafast dynamics of this system and found that this dyad exhibited both faster charge-separation and slower charge-recombination dynamics in the solid state relative to the solution state. The faster charge-separation dynamics were assigned to intermolecular electron-transfer dynamics, whilst the slower recombination dynamics were assigned to the migration of charge carriers to energetically more favourable sites within the film. We believe that the optimisation of photovoltaic devices based upon molecular donor–acceptor structures requires a detailed understanding of the correlation between molecular structure and electron-transfer dynamics of these structures in solid films. For this reason, we begin this report by making a detailed comparison of the charge-recombination dynamics of two molecular dyads, C_{60}–BN–exTTF (**1**) (BN = 1,1′-binaphthyl) and C_{60}–TVB–exTTF (**2**) (TVB = bisthienylvinylenebenzene), in which the donor (exTTF) and acceptor (C_{60}) units are connected by a chiral binaphthyl π-conjugated system. These dyads are investigated in both solution and solid films.

Figure 1 illustrates the chemical structures of the dyads used in this study, which differ only in the degree of conjugation of the molecular wire that connects both moieties. The use of tetrathiafulvalene and π-extended tetrathiafulvalene (exTTF) units is based on their strong electron-donating character and their thermodynamic stability when oxidised, which stems from the gain in aromaticity of the dicationic species.[24–33] Moreover, careful design of the molecular dyads has enabled us to prepare moieties with long alkyl side chains attached to the molecular bridge to allow high solubility in organic solvents for both systems. Furthermore, dyad **1** possesses a binaphthyl unit as molecular bridge, which breaks the molecular conjugation between donor and acceptor moieties.[34] In contrast, for dyad **2**, the π-orbital conjugation extends from the exTTF group to the C_{60} unit by using a bisthienylvinylenebenzene (*o*-1,4-dialkoxy-2,5-bis[2-(2-thienyl)vinyl]benzene) unit. We attempt to rationalise the different dynamics we observe in solution and solid films in terms of the molecular structures of the dyads and discuss these results in terms of the optimisation of dyad structures for photovoltaic device applications.

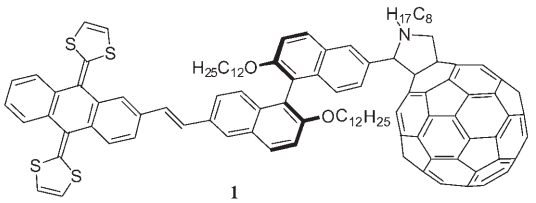

1

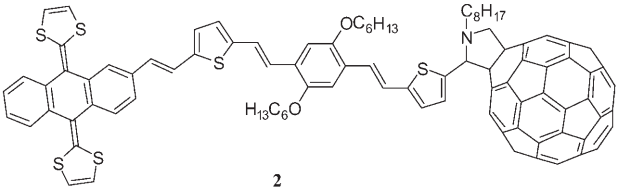

2

Figure 1. Chemical structures of C_{60}–BN–exTTF (dyad **1**) and C_{60}–TVB–exTTF (dyad **2**).

Experimental Section

Synthesis of molecular dyads

General: FTIR spectra were recorded with KBr pellets on a Nicolet-Magna-IR 5550 spectrometer. Electrospray ionization (ESI) mass spectra were recorded on a HP1100MSD spectrometer. UV/Vis spectra were recorded in dichloromethane using 1 cm quartz cuvettes on a Varian Cary 50 Scan spectrophotometer. NMR spectra were recorded on Bruker AC-200 (^{1}H, 200 MHz; ^{13}C, 50 MHz) and AMX-500 (^{1}H, 500 MHz; ^{13}C, 125 MHz) spectrometers at 298 K using partially deuterated solvents as internal standards. Chemical shifts are given as δ values (internal standard: TMS). Elemental analyses were performed on Perkin–Elmer 2400 CHN and 2400 CHNS/O analysers. Cyclic voltammograms were recorded on a potentiostat/galvanostat AUTOLAB with PGSTAT30 equipped with GPES software for Windows (version 4.8). A conventional three-compartment cell was used with a glassy carbon electrode (GCE) as the working electrode, a saturated calomel electrode (SCE) as the reference electrode, Pt wire as the counter electrode, Bu_4NClO_4 as the supporting electrolyte, an *o*-dichlorobenzene/acetonitrile (DCB/MeCN) solvent mixture (4:1 v/v), and a scan rate of 200 mV s^{-1} (also see Table 1 below).

Aldehyde ***9***: A mixture of the π-extended TTF derivative **8**[35] (112 mg, 0.15 mmol) and potassium *tert*-butoxide (34 mg, 0.3 mmol) was placed under reflux in dry toluene under an argon atmosphere for 30 minutes. Once the formation of the ylide was completed, a solution of 1,4-dihex-

yloxy-2,5-bis[(1*E*)-2′(5-formyl-2-tienyl)vinyl]benzene (**7**)[36] (117 mg, 0.22 mmol) in toluene (10 mL) was added in one portion and the mixture was reacted further under reflux conditions for 3 h. The crude product was cooled to room temperature and CH_3OH (5 mL) was added. After evaporation of the solvent mixture, the residue was purified by chromatography on silica gel with a hexane/CH_2Cl_2 (3:2) mixture as eluent to give the corresponding dyad as a red solid (63 mg, 45%). ^{1}H NMR (200 MHz, $CDCl_3$, 25°C, TMS): δ = 9.85 (s, 1H; −CHO), 7.81 (s, 1H), 7.73–7.65 (m, 4H), 7.50 (d, ^3J(H,H) = 16.4 Hz, 2H), 7.34 (d, ^3J(H,H) = 16.1 Hz, 1H), 7.33 (d, ^3J(H,H) = 16.5 Hz, 1H), 7.32 (m, 2H), 7.23 (d, ^3J(H,H) = 16.4 Hz, 2H), 7.14 (m, 2H), 7.04 (s, 2H), 6.94 (m, 3H), 6.32 (s, 4H), 4.05 (t, ^3J(H,H) = 6.2 Hz, 4H), 1.89 (m, 4H; $-CH_2-$), 1.55–1.15 (m, 4H), 1.25 (s, 4H), 0.88 ppm (m, 6H; $-CH_3$); ^{13}C NMR (50 MHz, $CDCl_3$, 25°C, TMS): δ = 182.47, 153.69, 151.70, 151.03, 142.76, 142.25, 141.26, 137.27, 135.88, 135.80, 135.30, 135.25, 134.82, 134.69, 128.29, 128.18, 127.94, 127.32, 127.23, 125.99, 125.35, 125.06, 124.96, 124.15, 123.33, 123.02, 122.60, 122.09, 121.90, 120.98, 117.27, 117.07, 111.13, 110.38, 69.62, 69.42, 31.65, 31.59, 29.44, 29.37, 25.95, 25.92, 22.68, 22.64, 14.11, 14.04 ppm; IR (KBr) $\tilde{\nu}$ = 2925, 2854, 1655, 1493, 1464, 1433, 1377, 1260, 1219, 1043, 943, 798, 635 cm^{-1}; UV/Vis (CH_2Cl_2): λ_{max} ($\log\varepsilon$) = 233 (4.60), 367 (4.40), 479 nm (4.80 mol^{-1} cm^3 dm^{-1}); MS (ESI): *m*/*z* (%): 949 (100) [*M*+Na]$^+$.

Dyad **2**: A mixture of the aldehyde **9** (45 mg, 0.049 mmol), [60]fullerene (35 mg, 0.049 mmol) and *N*-octylglycine (27 mg, 0.15 mmol) in chlorobenzene (28 mL) was placed under reflux for 24 hours. After cooling to room temperature, the crude product was purified by column chromatography on silica gel, using CS_2 to elute the unreacted fullerene, followed by a hexane/toluene (7:3) mixture to isolate compound **2** as a black solid (39 mg, 45%). M.p. 206–208°C (hexane/toluene); ^{1}H NMR (500 MHz, $CDCl_3$, 25°C, TMS): δ = 7.80 (d, ^3J(H,H) = 1.4 Hz, 1H), 7.70 (m, 2H), 7.67 (d, J = 8.0 Hz, 1H), 7.35 (dd, $^3J_1$(H,H) = 8.0 Hz, $^3J_2$(H,H) = 1.4 Hz, 1H), 7.30 (d, ^3J(H,H) = 3.4 Hz, 1H), 7.29 (d, ^3J(H,H) = 3.4 Hz, 2H), 7.23 (d, ^3J(H,H) = 16.5 Hz, 2H), 7.23–7.16 (m, 3H), 7.01 (s, 1H), 6.98 (d, ^3J(H,H) = 16.5 Hz, 2H), 6.96 (d, ^3J(H,H) = 16.5 Hz, 1H), 6.95 (d, ^3J(H,H) = 16.5 Hz, 1H), 6.94 (m, 1H), 6.31 (s, 4H), 5.33 (s, 1H), 5.08 (d, ^3J(H,H) = 9.6 Hz, 1H), 4.10 (d, ^3J(H,H) = 9.6 Hz, 1H), 4.02 (m, 4H), 3.43 (m, 1H), 2.62 (m, 1H), 1.87 (m, 6H), 1.55–1.25 (m, 22H), 0.93 ppm (t, 9H); ^{13}C NMR (125 MHz, $CDCl_3$, 25°C, TMS): δ = 156.19, 154.22, 153.38, 153.34, 151.13, 151.07, 147.32, 147.31, 146.94, 146.37, 146.31, 146.27, 146.19, 146.15, 146.12, 146.07, 145.94, 145.92, 145.78, 145.51, 145.50, 145.46, 145.42, 145.32, 145.28, 145.24, 145.15, 144.85, 144.71, 144.65, 144.38, 144.36, 143.15, 143.02, 142.96, 142.68, 142.56, 142.32, 142.23, 142.14, 142.07, 142.03, 141.96, 141.94, 141.90, 141.65, 141.59, 140.15, 140.12, 139.90, 139.73, 137.08, 136.69, 135.85, 135.80, 135.73, 135.56, 135.28, 135.24, 134.73, 129.02, 128.69, 128.21, 128.07, 127.34, 126.87, 126.43, 126.35, 125.98, 125.33, 125.29, 125.08, 124.96, 124.93, 124.13, 123.70, 123.63, 122.57, 122.43, 122.28, 122.08, 121.97, 117.32, 117.25, 117.10, 110.93, 110.48, 109.57, 78.49, 69.53, 69.45, 68.69, 66.97, 53.60, 53.40, 31.97, 31.65, 29.71, 29.45, 29.41, 29.35, 28.32, 27.56, 25.95, 22.73, 22.71, 22.69, 14.18, 14.13 ppm; IR (KBr): $\tilde{\nu}$ = 2946, 2920, 2851, 1635, 1541, 1451, 1183, 941, 752, 635, 526 cm^{-1}; UV/Vis (CH_2Cl_2): λ_{max} ($\log\varepsilon$) = 256 (5.21), 309 (4.76), 332 (4.77), 441 (4.92, sh), 468 nm (4.96 mol^{-1} cm^3 dm^{-1}); MS (ESI): 1773 (100) [*M*+H]$^+$.

Thin film preparation: All glass used for drop-casting of solutions was cleaned by using mixtures of acetonitrile/distilled water/isopropanol and sonicated for 30 minutes. After the cleaning step, the glass was dried at 120°C for 30 minutes to ensure removal of all solvents. Thin films were obtained from a diluted solution of each molecular dyad. Films were fabricated for a range of different solvents (dichloromethane, chlorobenzene, toluene and acetonitrile) and dyad concentrations ($1–15\times10^{-5}$ M) by employing both drop-casting and spin-coating methods. Optimum optical quality of the deposited films was obtained with dichloromethane. The kinetics of the transient optical data was found to be independent of dyad concentration, deposition technique and the use of sonication prior to film deposition. All data reported herein were obtained with films drop cast from dichloromethane with dyad concentrations of 1×10^{-5} M unless otherwise stated.

Optical transient studies: Nanosecond–microsecond transient spectroscopy experiments were performed by using a Xenon lamp as a probe source and a Nd-YAG laser as excitation source (λ_{ex} = 335 nm and pulse duration < 6 ns) at 1 Hz. The resulting photoinduced change in absorption was monitored by employing a 75 W Xenon arc lamp, a PTI model 101 monochromator (dual grating) after the sample, a TDS Tektronix 2022 digital storage oscilloscope and an Si-based photodiode (Costronics Electronics) as a photodetector. Data acquisition was carried out by using Tekave version 1.43 software. The UV/Vis spectra before and after the laser transient experiments were measured by using a double-beam Shimadzu UV-1601 spectrophotometer.

Results

Synthesis: Dyad **1** (exTTF–BN–C_{60}) was synthesized by following the method previously reported by our group.[34] Dyad **2** (exTTF–TVP–C_{60}) was obtained in a multistep synthetic procedure as depicted in Scheme 1. Thus, a twofold Wittig–Horner olefination reaction of bisphosphonate **3**[37] with commercially available 4-bromo-2-formylthiophene

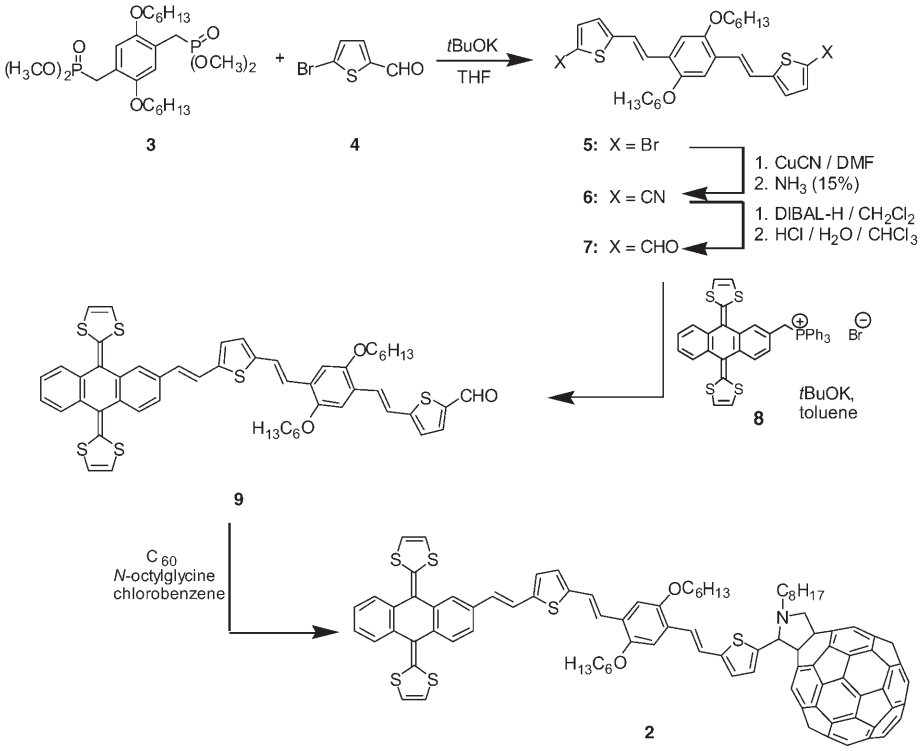

Scheme 1. Synthesis of the C_{60}–TVB–exTTF dyad (**2**).

under basic conditions afforded the π-conjugated compound **5** bearing two bromine atoms at terminal positions. A further Rosemund–von Braun reaction with copper(I) cyanide in DMF, followed by treatment with ammonia, led to the dicyano derivative **6**[38]. Compound **6** underwent a reduction process with DIBAL-H and hydrolysis to form dialdehyde **7**. A careful stoichiometric Wittig reaction of **7** with exTTF phosphonium salt **8**[36] afforded compound **9** bearing the exTTF unit and a suitable formyl group. This formyl group reacted with C_{60} in the presence of *N*-octyl glycine to form the final fulleropyrrolidine **2**, according to the Prato procedure,[39] by 1,3-dipolar cycloaddition of the azomethyne ylide, generated in situ, to the C_{60} molecule (Scheme 1).

Purification of **2** was accomplished by using flash chromatography (silica gel, CS_2 to recover unreacted C_{60}, then hexane/toluene 7:3) to obtain dyad **2** in 45% yield. The ^{1}H NMR spectrum (500 MHz) shows, in addition to the presence of the protons of exTTF and the pyrrolidine ring, the presence of the all-*trans* vinyl groups at $\delta = 7.23$, 6.98, 6.96 and 6.95 ppm ($J^3 \approx 16.5$ Hz, see the Experimental Section). The UV-visible spectrum of **2** shows that it consists of a simple superimposition of the constituent fragments, thus confirming the lack of significant electronic interactions between the electroactive species in the ground state.

Electrochemical characterisation: The electrochemical features of dyads **1** and **2** were probed by using cyclic voltammetry in solution at room temperature, and showed amphoteric redox behaviour with donor and acceptor electroactive responses. The redox potentials are collected in Table 1 with those of the parent exTTF, pristine C_{60} and the unsubstituted fulleropyrrolidine (Fp) for comparison (Table 1).

Table 1. Redox potential (E in V) values of novel compounds **1** and **2** and reference compounds.[a,b]

	E^1_{pa}	E^2_{pa}	E^3_{pa}	E^1_{pc}	E^2_{pc}	E^3_{pc}	E^4_{pc}	E^5_{pc}
exTTF	+0.55	–	–	–	–	–	–	–
C_{60}	–	–	–	−0.54	−0.96	−1.43	−1.92	–
Fp	–	–	–	−0.64	−1.03	−1.58	−1.99	–
1	+0.57	+1.04	+1.33	−0.64	−1.05	−1.60	−2.09	–
2	+0.50	+0.91	+1.29	−0.66	−1.07	−1.62	−1.87	−2.05

[a] Conditions: V versus SCE; working electrode, GCE; reference electrode, Ag/Ag^+; counter electrode, Pt; 0.1 M Bu_4NClO_4; scan rate, 200 mV s^{-1}; concentrations, 0.5–2.0 × 10^{-3} M; solvent, *o*DCB:MeCN (4:1 v/v). [b] E_{pa} and E_{pc} are anodic and cathodic peak potentials, respectively.

Similarly to dyad **1**,[34] dyad **2** shows the presence of four quasireversible one-electron reduction waves, which correspond to the reduction of the fullerene core at −0.66, −1.07, −1.62 and −2.05 V. These values are cathodically shifted relative to pristine C_{60} and have been explained in terms of the saturation of a double bond of the fullerene core, which raises the LUMO energy. These values are furthermore quite similar to those found for the unsubstituted fulleropyrrolidine (Fp). However, in contrast to dyad **1**, another reduction wave is observed in dyad **2** at −1.87 V, which is assigned to the reduction of the π-conjugated bridge (see Figure 2). On the oxidation side, important differences are found between dyads **1** and **2**. Thus, dyad **1** shows a first

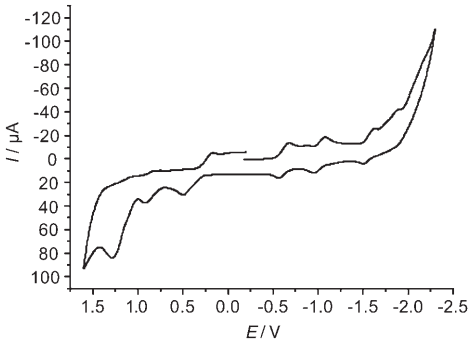

Figure 2. Cyclic voltammograms for dyad **2** at room temperature (solvent, *o*DCB/MeCN 4:1 v/v; supporting electrolyte, Bu_4NClO_4, scan rate, 200 mV s^{-1}).

quasireversible oxidation wave corresponding to the formation of the dication of the exTTF unit at +0.57 V, with two additional waves at +1.04 and +1.33 V stemming from the BN moiety. Dyad **2** also exhibits the quasireversible oxidation wave of the exTTF unit and two further oxidation waves corresponding to the π-conjugated bridge (TVB). However, the first oxidation potential value in **2** is significantly shifted towards less positive values relative to the parent exTTF (Table 1). This cathodic shift is in contrast to that observed for dyad **1** and reveals the better electronic communication existing between the exTTF unit and the C_{60} moiety through the π-conjugated bridge in dyad **2**. This finding is in agreement with the behaviour previously observed for the related C_{60}–TVB dyads, which also showed a small but noticeable electronic interaction between the π-conjugated oligomer and C_{60}.[38]

Behaviour in solution: First we consider the behaviour of dyads **1** and **2** in solution. Figure 3 shows the absorption spectra of both dyads in solution (black lines). As expected, both molecular dyads exhibit a strong absorption maximum in the blue spectral region, with the absorption maximum of dyad **2** redshifted relative to that of dyad **1** ($\lambda_{abs} = 465$ and 434 nm, respectively), consistent with the expected greater delocalisation of the π orbitals for this dyad.

The primary function of the molecular wire bridge in the dyads is to allow photoinduced electron transfer from the exTTF donor unit to the C_{60} electron-accepting molecule, thereby resulting in a long-lived charge-separated radical-pair state. We herein employ transient absorption spectroscopy to monitor these electron-transfer dynamics by focusing, in particular, upon the lifetime of the charge-separated state. A long lifetime of this state is essential for photovoltaic device function, allowing efficient charge collection by the device electrodes. Figure 4 compares typical data for both dyads in solution, with Figure 5 showing the transient ab-

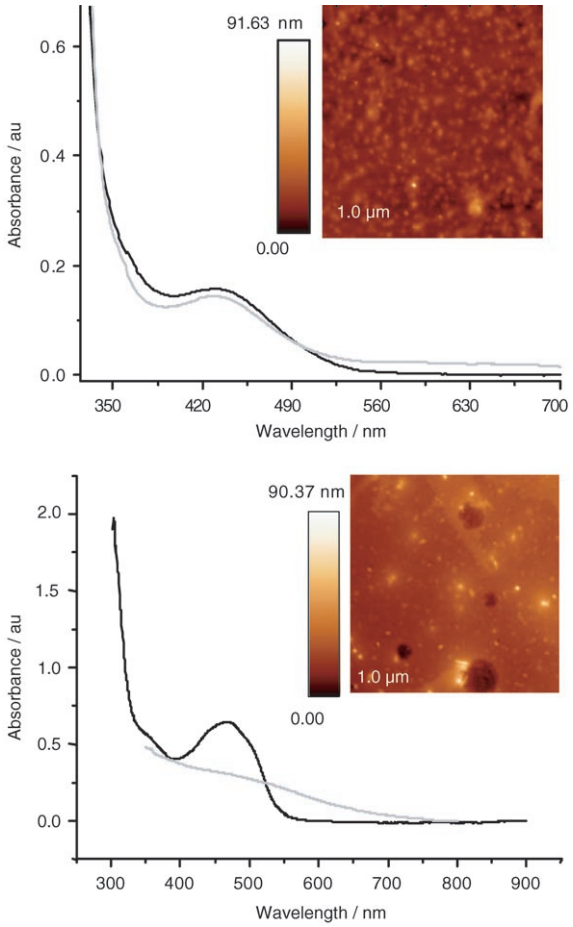

Figure 3. The UV-visible spectra of dyad **1** (top) and dyad **2** (bottom) in dichloromethane (black curves) and film (grey curves), spin coated on transparent glass. The insets show the AFM images of the films. Note the AFM and the optical spectra both indicate an aggregated, more scattered film for dyad **2** relative to **1**.

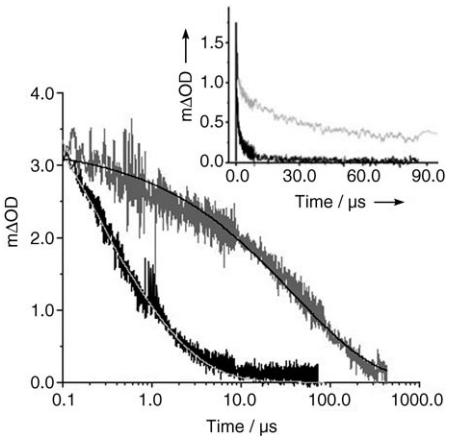

Figure 4. Log–linear plot for the electron-recombination dynamics for dyads **1** (grey) and **2** (black) in dichloromethane at $\lambda_{probe}=830$ and $\lambda_{ex}=355$ nm, with their representative stretched exponential fits. The inset shows the linear–linear plot.

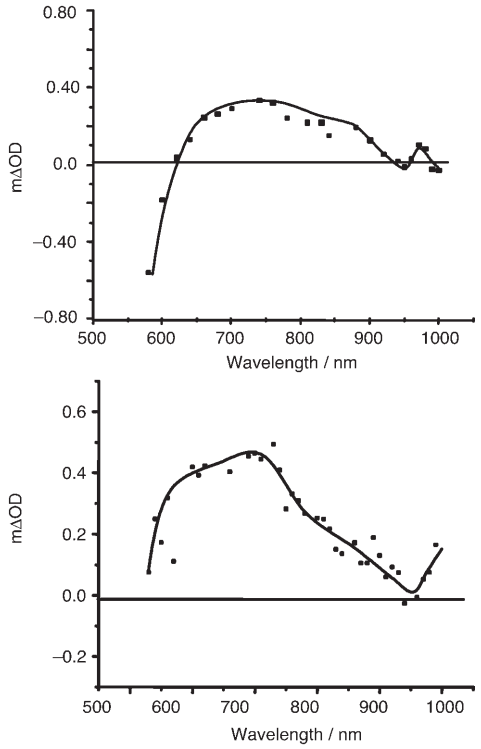

Figure 5. Transient absorption spectra ($\lambda_{ex}=355$ nm) recorded after $t=1$ μs for dyad **1** in dichloromethane (top) and on thin film (bottom). The spectra show the features corresponding to exTTF$^{\bullet+}$ ($\lambda\approx700$ nm) and $C_{60}^{\bullet-}$ ($\lambda\approx980$ nm) for both samples.

sorption spectrum observed one microsecond after pulsed laser excitation at $\lambda_{ex}=355$ nm.

Both dyads **1** and **2** show the expected formation of an exTTF radical cation (exTTF$^{\bullet+}$)/C_{60} radical anion ($C_{60}^{\bullet-}$) charge-separated state. In both cases, photoinduced absorption maxima are observed at $\lambda\approx700$ nm, assigned to the exTTF$^{\bullet+}$ species, and at $\lambda\approx980$ nm, assigned to the $C_{60}^{\bullet-}$ species. These values are consistent with previous observations.[12]

Typical spectra for charge recombination of the exTTF$^{\bullet+}$/$C_{60}^{\bullet-}$ state in solution are shown in Figure 5, monitored at $\lambda\approx980$ nm (assigned to the $C_{60}^{\bullet-}$ absorption). It is apparent that the decay dynamics of **1** are retarded compared with those of **2**, with decay lifetimes, $t_{50\%}$, of $\tau=25$ and 0.7 μs, respectively. This retardation is consistent with the expected less-conjugated character of the molecular bridge of dyad **1**. The faster recombination for dyad **2** results from the extended conjugation of the molecular bridge "wiring" the donor and acceptor species, thereby enhancing the electronic coupling between these species.

For both dyads, the recombination dynamics are nonexponential, as is apparent from their dispersive appearance on the logarithmic timescale employed. Numerical fitting of the decay dynamics to a stretched exponential function ($\Delta OD \propto \exp(-(t/\tau)^{\alpha})$ gave reasonable fits to the data, with stretch parameter $\alpha\approx0.45$ for both dyads. This nonexponential behaviour is tentatively assigned to different structural conforma-

tions of the dyads, as discussed in more detail below. Furthermore, we would like to point out that despite the use of diluted solutions (1×10^{-5} M) for both dyads, we still observed aggregation processes for dyad **2**. This behaviour implies that, although experimental conditions are identical for both samples, the nature of the molecular bridge influences the formation of aggregates.

Behaviour in the solid state: We now turn to the investigation of molecular films fabricated by drop casting dyads **1** and **2** onto glass substrates from solution. For dyad **1**, the ground-state absorption spectra in solution and in the solid film were indistinguishable, indicating that exTTF π orbitals involved in the optical absorption were not strongly perturbed in the film relative to their state in solution. The optical quality of the films formed with dyad **2** was found to be poorer than that for dyad **1**, resulting in significant light scattering and preventing the determination of a precise absorption spectrum for this dyad in the solid film. The pronounced light scattering of films fabricated from dyad **2** is attributed to the formation of molecular aggregates, as discussed below.

Figure 6 compares transient absorption data obtained for dyad **1** in solution and as a solid film. For such film studies, it is essential to address the excitation-density dependence of the transient data. For isolated molecules in solution, the transient kinetics are expected to be excitation-density independent. However, for solid films, nonlinear effects due to polaron–polaron, exciton–exciton or exciton–polaron interactions can arise at higher excitation densities, resulting in excitation-density-dependent dynamics and complicating interpretation of the experimental data. For this reason, transient absorption data were collected as a function of excitation density. Figure 6 (top) compares dynamics for solution and solid films at two (high and low) excitation densities, whilst Figure 6 (bottom) shows the dependence of the amplitude of the transient signal on laser intensity for both samples. Most importantly, it is apparent that the recombination dynamics for the solid film are approximately tenfold faster than those observed in solution (lifetimes of $\tau=2.1$ and 25 μs). It is furthermore apparent that the charge-recombination kinetics for both the solution and film are independent of excitation density over the range studied. The magnitude of the transient signal exhibits a linear dependence on excitation density for the solution data as expected, but a sublinear behaviour for the solid film. At low excitation densities, the magnitude of the transient absorption signal for both samples are indistinguishable within error margins, indicating a similar yield of long-lived charge-separated states. However, at higher laser intensities, the amplitude of the signal for the film data starts to become saturated, indicating a lower yield of such states.

An analogous comparison of solution and film data was undertaken for dyad **2**, as shown in Figure 7. Most strikingly, and in marked contrast to dyad **1**, it is apparent that the recombination dynamics for the solid film are an order of magnitude *slower* than those observed in solution (lifetimes

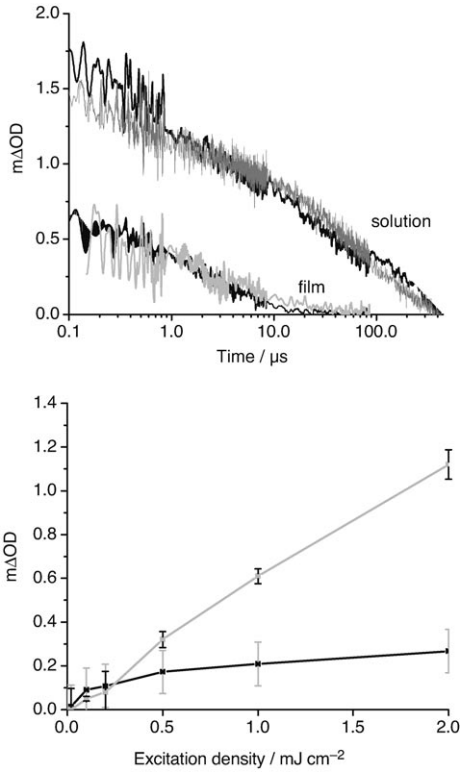

Figure 6. Top: Comparison of the electron recombination dynamics at high (black line) and low (grey line) excitation density for a solution (in dichloromethane) and film of dyad **1**. The signals have been normalised to clearly exhibit the dynamics ($t=0.1$ μs). Bottom: Laser-power dependence of the transient absorption signal for dyad **1** ($\lambda_{probe}=830$ and $\lambda_{ex}=355$ nm); grey line = film, black line = solution.

of $\tau=7$ and 0.7 μs, respectively). These dynamics are again observed to be nonexponential and independent of excitation density. The magnitude of the transient signal is observed to exhibit a sublinear dependence upon excitation density, both for the solution and solid film data. This behaviour is in contrast to that of dyad **1**, in which such behaviour was only observed in the solid film (absolute comparison of the film and solution signal magnitude for this dyad was not possible due to the scattering nature of the solid film).

Discussion

The faster recombination dynamics observed in solution for the more conjugated dyad (**2**) is consistent with the expected stronger electronic coupling through the molecular bridge for this dyad. However, the nonexponential nature of the dynamics is unexpected. Most plausibly, this nonexponential behaviour arises from different structural conformations of the dyad in solution, varying the electronic coupling between the $exTTF^{\bullet+}$ and $C_{60}^{\bullet-}$ species. For dyad **1**, the magnitude of the transient signal exhibits the expected linear dependence on excitation density, consistent with negligible dyad–dyad interactions. However, for dyad **2**, the transient signal exhibits a sublinear dependence on excitation density,

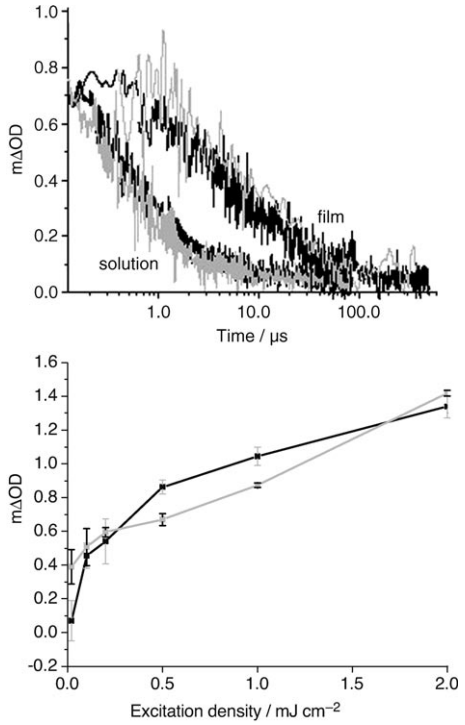

Figure 7. Top: Comparison of the electron recombination dynamics at high (black line) and low (grey line) excitation density for a solution (in dichloromethane) and film of dyad **2**. The signals have been normalised to clearly exhibit the dynamics ($t = 0.1$ μs). Bottom: Laser-power dependence of the transient absorption signal for dyad **2** ($\lambda_{probe} = 830$ and $\lambda_{ex} = 355$ nm); grey line = film, black line = solution.

tending to saturate in magnitude as the excitation density was increased. This behaviour was observed in both concentrated (≈0.06 mM) and dilute (0.01 mM) solutions. This nonlinear behaviour suggests significant dyad–dyad interactions (for example, exciton–exciton annihilation or bimolecular recombination processes), indicative of significant dyad aggregation even in dilute solution. Such aggregation is consistent with the scattering nature of the solid films fabricated with this dyad, and further supported by atomic force microscopy (AFM) studies of the solid films for both dyads. We believe that dyad **2** might show a higher degree of molecular ordering than dyad **1** by π–π stacking between the fully conjugated molecular bridges. These molecular aggregates were previously demonstrated for other systems in which the presence of conjugated units induced ordered structures. For this reason, the presence of molecular aggregation is tentatively attributed to the more planar and conjugated nature of dyad **2** relative to dyad **1**.

For dyad **1**, the recombination dynamics observed for the solid film are approximately ten times faster than those observed in solution. In solution, these recombination dynamics are assigned to geminate, monomolecular charge recombination of exTTF$^{\bullet+}$/$C_{60}^{\bullet-}$ radical pairs in isolated dyad molecules, consistent with the observed excitation-density dependence. The observed excitation-density independence of the recombination dynamics in the solid film suggests that the faster recombination dynamics observed for solid films cannot be attributed to bimolecular recombination processes. Rather, the accelerated recombination dynamics are assigned to stronger electronic coupling between exTTF$^{\bullet+}$ and $C_{60}^{\bullet-}$ geminate radical pairs in the film. Such stronger coupling may result from enhanced intramolecular electronic coupling within each dyad owing, for example, to a more favourable structural conformation or to strong intermolecular interactions between an exTTF moiety on one dyad and a C_{60} moiety on a neighbouring dyad. In either case, the resulting fast recombination dynamics suggest that this dyad will not be attractive for photovoltaic device applications. On the other hand, for dyad **2**, it is striking that the recombination dynamics are observed to be ten times *slower* in the solid film relative to solution. This retardation is consistent with a recent study of Janssen et al. of OPV–C_{60} dyads in solution and solid films.[23] It is possible that the recombination dynamics for dyad **2** also originate from geminate recombination processes, as discussed above for dyad **1**, but with reduced rather than increased electronic coupling in the film relative to the solution. However, both the lower dielectric constant expected for films compared with solutions ($\varepsilon_r \approx 3$–4 in film compared with 9 in solution),[40,41] and the more dense molecular packing in the film, suggest that the electronic coupling for solid films should be higher rather than lower than that in solution, contrary to this interpretation. More plausibly, the slow recombination dynamics observed in the solid film can be assigned to dissociation of the photogenerated radical pairs to free carriers, and subsequent trapping of these free carriers on low-energy sites within the film. Such a model of slow, detrapping-limited recombination dynamics would be consistent with studies of random polymer–C_{60} blends, both carried out by us and other groups. This interpretation requires dissociation of the geminate radical pairs, in contrast to dyad **1**, where the experimental data is consistent with geminate charge-recombination dynamics, both in solution and the solid film. Enhanced dissociation of geminate radical pairs for dyad **2** is consistent with the expected greater π-orbital stacking of this dyad, as evidenced by the dyad aggregation observed even in solution. The enhanced radical-pair dissociation and slow charge-recombination dynamics can be expected to favour efficient photovoltaic device function, although we note that the poor optical quality of the spun coated films in practice limit device applications for this dyad.

Efficient photovoltaic device function requires the photogeneration of a high yield of long-lived charge-separated species. On the basis of solution dynamics alone, dyad **1** appears most attractive for such applications. However, it is apparent from the experimental data reported here that such solution data cannot be readily extrapolated to solid films. After consideration of the charge-recombination dynamics observed in solid films, it is apparent that the electron-transfer dynamics for dyad **2** are in fact more suitable for photovoltaic applications. Several factors influence the electron-transfer dynamics in the solid film which are not present in solution. Firstly, donor–acceptor electronic coupling may be very different in solution and in solid films. A

key concern here is the potential for intermolecular interactions between a donor on one molecule and an acceptor on a neighbouring species. Long geminate radical-pair lifetimes may therefore require consideration of not only intramolecular but also intermolecular electronic interactions. A second consideration is the efficiency of geminate radical-pair dissociation to yield free carriers, requiring favourable intermolecular acceptor–acceptor and/or donor–donor interactions. The success of dyad **2** relative to dyad **1** in generating long-lived charge-separated species in solid films, as reported here, appears to derive primarily from this latter consideration, with π-orbital stacking favouring efficient radical-pair dissociation.

Conclusion

The application of molecular donor–acceptor structures to photovoltaic energy conversion requires a detailed understanding of the correlations between molecular structure, electron-transfer dynamics and device function. More detailed studies, including different temperatures during thin-film formation, will be necessary to completely understand the charge-transfer process at interfaces in organic molecular devices. It can be concluded from the studies reported here that transient absorption studies of solid molecular films is a powerful approach to elucidating such correlations, and may play an effective role in guiding future optimisation of molecular structure for such applications.

Acknowledgements

We would like to acknowledge financial support from BP Solar (British Petroleum), the Engineering and Physical Sciences Research Council (EPSRC) and the Ministerio de Ciencia y Tecnología of Spain (project BQU2002-00855). E.P. would like to acknowledge the EU for the Marie Curie Fellowship HPMF-CT-2002-01744 for financial support and the MEC for the Ramon y Cajal Fellowship.

[1] F. Padinger, R. S. Rittberger, N. S. Sariciftci, *Adv. Funct. Mater.* **2003**, *13*, 85.
[2] M. R. Wasielewski, *Chem. Rev.* **1992**, *92*, 435.
[3] D. Gust, T. A. Moore, A. L. Moore, *Acc. Chem. Res.* **2001**, *34*, 40.
[4] H. Imahori, Y. Mori, *J. Photochem. Photobiol. C* **2003**, *4*, 51.
[5] R. Holzwarth, M. Katterle, M. G. Muller, Y. Ma, V. Prokhorenko, *Pure Appl. Chem.* **2001**, *73*, 469.
[6] P. Samorì, X. Yin, N. Tcheborateva, Z. Wang, T. Pakula, F. Jackel, M. D. Watson, A. Venturini, K. Mullen, J. P. Rabe, *J. Am. Chem. Soc.* **2004**, *126*, 3567.
[7] a) K. G. Thomas, V. Biju, P. V. Kamat, M. V. George, D. M. Guldi, *ChemPhysChem* **2003**, *4*, 1299; b) F. Giacalone, J. L. Segura, N. Martín, D. M. Guldi, *J. Am. Chem. Soc.* **2004**, *126*, 5340.
[8] a) I. B. Martini, B. Ma, T. Da Ros, R. Hegelson, F. Wudl, B. J. Schwartz, *Chem. Phys. Lett.* **2000**, *327*, 253; b) G. De la Torre, F. Giacalone, J. L. Segura, N. Martín, D. M. Guldi, *Chem. Eur. J.* **2005**, *11*, 1267.
[9] A. Harriman, *Angew. Chem.* **2004**, *116*, 5093; *Angew. Chem. Int. Ed.* **2004**, *43*, 4985.
[10] S. C. J. Meskers, P. A. van Hal, A. J. H. Spiering, A. F. G. van der Meer, J. C. Hummelen, R. A. J. Janssen, *Phys. Rev. B* **2000**, *61*, 9917.
[11] K. Ohkubo, H. Kotani, J. Shao, Z. Ou, K. M. Kadish, G. Li, R. Pandey, M. Kujitsuka, O. Ito, H. Imahori, S. Fukuzumi, *Angew. Chem.* **2004**, *116*, 871; *Angew. Chem. Int. Ed.* **2004**, *43*, 853.
[12] G. Steinberg-Yfrach, J. L. Rigaudt, E. N. Durantini, A. L. Moore, D. Gust, *Nature* **1998**, *392*, 479.
[13] N. Armaroli, F. Barigelletti, P. Ceroni, J. F. Eckert, J. F. Nicoud, J. F. Nierengarten, *Chem. Commun.* **2000**, 599.
[14] J. F. Nierengarten, J. F. Eckert, J. F. Nicoud, L. Ouali, V. Krasnikov, G. Hadziioannou, *Chem. Commun.* **1999**, 617.
[15] J. F. Eckert, J. F. Nicoud, J. F. Nierengarten, S. G. Liu, L. Echegoyen, F. Barigelletti, N. Armaroli, L. Ouali, V. V. Krasnikov, G. Hadziioannou, *J. Am. Chem. Soc.* **2000**, *122*, 7467.
[16] E. Peeters, P. A. van Hal, J. Knol, C. J. Brabec, N. S. Sariciftci, J. C. Hummelen, R. A. J. Janssen, *J. Phys. Chem. B* **2000**, *104*, 10174.
[17] J. L. Segura, R. Gómez, N. Martín, C. Luo, A. Swartz, D. M. Guldi, *Chem. Commun.* **2001**, 707.
[18] P. A. van Hal, R. A. J. Janssen, G. Lanzani, G. Cerullo, M. Zavelani-Rossi, S. De Silvestri, *Phys. Rev. B* **2001**, *64*, 075206.
[19] N. Armaroli, G. Accorsi, J.-P. Gisselbrecht, M. Gross, V. Krasnicov, D. Tsamouras, G. Hadziioannou, M. J. Gómez-Escalonilla, F. Langa, J. F. Eckert, J. F. Nierengarten, *J. Mater. Chem.* **2002**, *12*, 2077.
[20] J. F. Nierengarten, N. Armaroli, G. Accorsi, Y. Rio, J. F. Eckert, *Chem. Eur. J.* **2003**, *9*, 37.
[21] T. Gu, J. F. Nierengarten, *Tetrahedron Lett.* **2001**, *42*, 3175.
[22] T. Gu, D. Tsamouras, C. Melzer, V. Krasnikov, J.-P. Gisselbrecht, M. Gross, G. Hadziioannou, J. F. Nierengarten, *ChemPhysChem* **2002**, *3*, 124.
[23] P. A. van Hal, S. C. J. Meskers, R. A. J. Janssen, *Appl. Phys. A* **2004**, *79*, 41.
[24] N. Martín, L. Sánchez, C. Seoane, E. Ortí, P. M. Viruela, R. Viruela, *J. Org. Chem.* **1998**, *63*, 1268.
[25] *Fundamentals and Applications of Tetrathiafulvalene, Vol. 16* (Eds.: J. Yamada, T. Sugimoto), Springer, Berlin, **2004**.
[26] N. Martín, L. Sánchez, D. M. Guldi, *Chem. Commun.* **2000**, 113.
[27] M. A. Herranz, B. Illescas, N. Martín, C. Luo, D. M. Guldi, *J. Org. Chem.* **2000**, *65*, 5728.
[28] D. M. Guldi, L. Sánchez, N. Martín, *J. Phys. Chem. B* **2001**, *105*, 7139.
[29] M. A. Herranz, N. Martín, J. Ramey, D. M. Guldi, *Chem. Commun.* **2002**, 2968.
[30] S. Gonzalez, N. Martín, D. M. Guldi, *J. Org. Chem.* **2003**, *68*, 779.
[31] S. González, N. Martín, A. Swartz, D. M. Guldi, *Org. Lett.* **2003**, *5*, 557.
[32] M. C. Díaz, M. A. Herranz, B. M. Illescas, N. Martín, N. Godbert, M. R. Bryce, C. Luo, A. Swartz, G. Anderson, D. M. Guldi, *J. Org. Chem.* **2003**, *68*, 7711.
[33] M. C. Díaz, B. M. Illescas, N. Martín, P. M. Viruela, R. Viruela, E. Ortí, O. Brede, I. Zilbermann, D. M. Guldi, *Chem. Eur. J.* **2004**, *10*, 2067.
[34] D. M. Guldi, G. de la Torre, F. Giacalone, J. L. Segura, N. Martín, *Chem. Eur. J.* **2005**, *44*, 1267.
[35] L. Sánchez, I. Pérez, N. Martín, D. M. Guldi, *Chem. Eur. J.* **2003**, *9*, 2457.
[36] D. M. Guldi, C. Luo, A. Swartz, R. Gómez, J. L. Segura, N. Martín, *J. Phys. Chem. B* **2004**, *108*, 455.
[37] U. Stalmach, H. Kolshorn, I. Brehm, H. Meier, *Liebigs Ann.* **1996**, 1449.
[38] D. M. Guldi, C. Luo, A. Swartz, R. Gómez, J. L. Segura, N. Martín, C. J. Brabec, N. S. Sariciftci, *J. Org. Chem.* **2002**, *67*, 1141.
[39] M. Maggini, M. Prato, G. Scorrano, *J. Am. Chem. Soc.* **1993**, *115*, 9798.
[40] J. A. Riddick, W. B. Bunger, *Organic Solvents*, Wiley, New York, **1970**.
[41] K. R. Seddon, A. Stark, M. J. Torres, *Pure Appl. Chem.* **2000**, *72*, 2275.

Received: December 20, 2004
Revised: August 5, 2005
Published online: October 27, 2005

